Journal of Sound and Vibration 576 (2024) 118296

Contents lists available at ScienceDirect

Journal of Sound and Vibration

journal homepage: www.elsevier.com/locate/jsvi

Shear flow effects in a 2D duct: Influence on wave propagation and direct impedance eduction

Jinyue Yang [a,*], Thomas Humbert [a], Joachim Golliard [a,b], Gwénaël Gabard [a]

[a] Laboratoire d'Acoustique de l'Université du Mans (LAUM), UMR 6613, Institut d'Acoustique - Graduate School (IA-GS), CNRS, Le Mans Université, France

[b] CTTM, 20 rue Thalès de Milet, 72000 Le Mans, France

ARTICLE INFO

Keywords:
Shear-flow effect
Impedance eduction
Acoustic liner
Duct acoustics

ABSTRACT

Impedance eduction of acoustic liners with flow is commonly performed under the assumption of a uniform velocity profile. In practice, the flow profile is not uniform and a significant mean flow shear is present close to the duct wall. The present paper aims to assess the validity of the uniform flow assumption, and more generally to study the effect of the mean flow shear on the impedance eduction process. This is particularly relevant when considering large ducts, high frequencies, high-order acoustic modes and flow velocities representative of aircraft engine nacelles. A numerical mode-matching model is used to compute the sound field in a 2D lined duct with different flow profiles. A detailed parametric study evaluates the influence of the mean flow shear on the axial wavenumbers of the acoustic modes and on the educed impedance. Various parameters are considered: the flow velocity profile (boundary layer thickness and mean Mach number), the direction of acoustic propagation relative to the flow, two different liner configurations and the presence of noise in the pressure data. A number of recommendations are given to achieve robust impedance eduction in large-duct facilities and at high-frequencies.

1. Introduction

Acoustic liners are widely used to reduce noise emissions from aircraft engines. Understanding their behaviour under realistic conditions is crucial for their development and design. A recent trend is to use impedance eduction to characterise acoustic liners in the presence of flow. These techniques can be broadly classified into two main categories: inverse and direct methods.

An inverse eduction method is an optimisation process that involves minimising the difference between acoustic quantities in the experimental and simulated fields, such as scattering matrix [1], insertion loss [2], acoustic pressure [3], acoustic wavenumber [4], etc. Various models can be used to simulate the acoustic field, such as the Convected Helmholtz Equation (CHE) [5], the Linearized Euler Equations (LEE) [5] and the Linearized Navier–Stokes Equations (LNSE) [6].

In contrast to the iterative process in the inverse method, direct methods only require a one-off calculation using a direct relationship between the axial wavenumber k_x and the liner impedance Z. The wavenumber is calculated from acoustic pressure measurements provided by a microphone array. The majority of direct impedance eduction methods [7–10] rely on the assumption of a uniform mean flow and the Ingard–Myers impedance condition [11,12], whereas others assume a sheared mean flow and use the Pridmore Brown Equation [13,14].

Considering a sheared flow, published results indicate that the assumption of uniform flow may introduce errors in the impedance results. A comparative study in the NASA GFIT [5] showed that differences would occur between the eduction results using the

* Corresponding author.
E-mail address: jinyue.yang.etu@univ-lemans.fr (J. Yang).

https://doi.org/10.1016/j.jsv.2024.118296
Received 4 August 2023; Received in revised form 15 December 2023; Accepted 21 January 2024
Available online 22 January 2024

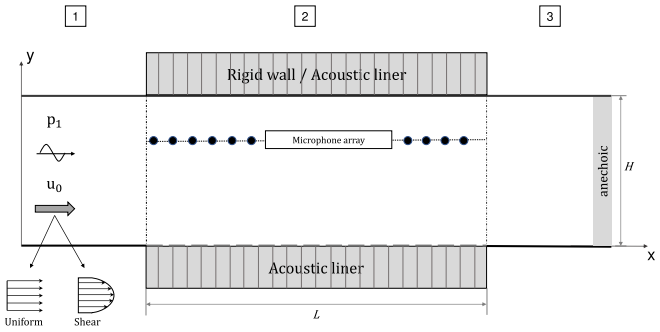

Fig. 1. Schematic of the 2D duct with a lined section.

assumptions of uniform and shear flow, and could be greater at higher Mach numbers. More recently, Jing et al. [14] exploited a straightforward method for impedance eduction in the presence of shear flow and boundary layer effects, and showed that the eduction was not susceptible to the exact shape of boundary layer, similar to the conclusion in [15]. Roncen et al. [16] evaluated the uncertainties on the flow profile in the modal decomposition based on Bayesian inference. They concluded that the uniform flow assumption did not introduce significant errors when considering only one mode propagation, and suggested more exploration on the impact of the use of the uniform flow assumption when considering multiple mode propagation. Subsequently, they noted that an apparent mismatch between wavenumber definitions appeared when considering a uniform mean flow [4]. However, when considering a larger duct, Spillere et al. [17] noted that the educed impedance was affected when considering a more realistic flow profile, which differs from the previous observations. Consequently, some questions remain: to what extent does the mean flow shear alter the impedance eduction? Is this effect influenced by other parameters such as duct size, frequency, flow velocity?

Most of experimental research focused on small cross-section ducts, while studies on the effect of shear flow in large ducts are limited. An existing study on large ducts is in the NASA CDTR [8,9]. The investigation showed similar impedance eduction results in a duct with small cross-section (the GFIT) and in a large-scale duct (the CDTR) when using the uniform flow assumption. The only discrepancies observed between the two ducts were at the very low, or very high, frequencies. This was explained by the low attenuation and the appearance of a higher-order mode, respectively [9]. While these experimental data provides useful information on the differences observed between small and large ducts, the impact of the mean flow shear on the eduction method remains to be more precisely assessed.

The present study aims to investigate the influence of the mean flow shear on the direct impedance eduction method, especially in the condition of large ducts and flow velocities representative of turbofan nacelles. For this purpose, we examine the effects of shear flow in two ways, first by assessing the change in the acoustic field and then by considering the eduction results. In addition, we develop and validate a double-liner configuration to improve the eduction performance in large ducts and with measurement noise. Section 2 introduces the numerical methods used to compute the acoustic field in 2D ducts and to calculate the liner impedance, considering both single- and double-liner configurations, assuming either a uniform flow or a sheared flow. In Section 3, a parametric analysis studies the effects of shear flow on the acoustic propagation and on the applicability of the uniform flow assumption when calculating the impedance from the wavenumber. Then, Section 4 presents the applications of these methods to numerical simulations of the impedance eduction method. Conclusions are outlined in Section 5.

2. Numerical methodology

This section starts by describing the numerical models used to calculate the sound fields in a 2D duct with either uniform or sheared mean flows. Then, these models are modified to compute the wall impedance from the knowledge of the axial wavenumbers of the sound field.

2.1. Calculation of a 2D acoustic field

We consider a 2D duct composed of three sections, as shown in Fig. 1. The first and third sections have hard walls, while the walls of the middle section can be treated with a locally reacting liner (either both the upper and lower walls, or only the lower wall). The height of the duct is denoted H and the length of the lined section is L. The axial coordinate is denoted x and y is the vertical coordinate. A single incident duct mode is propagating toward the liner from the left-hand side. The duct exit on the right-hand side is considered anechoic. A collection of pressure points mimicking the presence of a linear array of microphones will be used in the last part of the paper to perform numerical impedance eduction, which corresponds to the realistic case where the microphones are mounted on the lateral wall. The next sections introduce the propagation models, including either a uniform flow or a parallel sheared flow. These models are for linear acoustic waves with an implicit time dependence given by $e^{+i\omega t}$ where ω is the angular frequency.

2.1.1. Uniform flow case

We first assume that the duct contains a uniform axial flow with mean velocity u_0, density ρ_0 and sound speed c_0. In this case, the acoustic pressure $p(x, y)$ in the duct is governed by the convected Helmholtz equation:

$$\frac{1}{c_0^2}\frac{\mathrm{D}_0^2 p}{\mathrm{D}t^2} - \nabla^2 p = 0, \tag{1}$$

where $\mathrm{D}_0/\mathrm{D}t = \partial/\partial t + u_0\partial/\partial x$ is the material derivative associated to the mean flow. The boundary condition for a rigid wall is

$$\frac{\partial p}{\partial n} = 0, \tag{2}$$

indicating that the normal particle velocity vanishes at the duct wall. In the case of a lined wall, the Ingard–Myers boundary condition is used [12]:

$$\frac{\partial p}{\partial n} = -\frac{\mathrm{D}_0^2}{\mathrm{D}t^2}\frac{p}{\mathrm{i}\omega c_0 Z}, \tag{3}$$

where Z is the specific surface impedance (i.e. normalised by $\rho_0 c_0$) and n is the outward unit normal to the wall.

In each section of the duct, the acoustic pressure can be sought in the following modal form:

$$p(x, y) = \sum_n A_n^+ \Psi_n^+(y)\mathrm{e}^{-\mathrm{i}k_{xn}^+ x} + \sum_n A_n^- \Psi_n^-(y)\mathrm{e}^{-\mathrm{i}k_{xn}^- x}, \tag{4}$$

where each mode is defined by an amplitude $A_n^\pm$, a shape function $\Psi_n^\pm$ and an axial wavenumber $k_{xn}^\pm$. The wavenumbers and shape functions are solutions of an eigenvalue problem obtained from Eq. (1)–(3) and assuming solutions of the form $p = \Psi(y)\mathrm{e}^{-\mathrm{i}k_x x}$. For a rigid-wall section, this eigenvalue problem can be solved analytically, and the mode shape function is given by

$$\Psi_n(y) = \cos\left(n\pi\frac{y}{H}\right). \tag{5}$$

For a lined section, this problem is solved using a pseudo-spectral method [18]. More precisely, the pressure field is approximated using a basis of N Chebyshev polynomials and the differential equation is solved at $N-2$ Chebyshev points along the y axis. The resulting linear system is then closed using the two boundary conditions.

Once the modal basis is known in each section, the acoustic propagation in the whole duct is modelled using a mode-matching method [19]. This allows computing the modal amplitudes $A_n^\pm$ in each section, based on the conservation of mass and momentum.

The results shown in this paper have been checked for convergence with respect to N and to the number of duct modes used in the mode-matching scheme.

2.1.2. Shear flow case

Two common models used to describe sound propagation in parallel shear flows are the Linearised Euler Equations (LEEs) or the Pridmore Brown equation. An issue is that the gradient $u_0'(y)$ of the mean flow profile appears in these equations. For some common flow profiles, such as the inverse law profile [17], this velocity gradient tends to infinity at the duct wall, which can create difficulties for the numerical solutions. To avoid this issue, we introduce the vertical acoustic displacement ξ which is related to the vertical acoustic velocity v by $D_0\xi/Dt = v$. The LEEs can then be written as follows in terms of p and ξ:

$$\frac{\partial p}{\partial y} + \rho_0\frac{D_0^2\xi}{Dt^2} = 0, \tag{6a}$$

$$\rho_0 c_0^2\frac{D_0^2}{Dt^2}\frac{\partial \xi}{\partial y} - c_0^2\frac{\partial^2 p}{\partial x^2} + \frac{D_0^2 p}{Dt^2} = 0. \tag{6b}$$

It can be seen that the gradient of the mean flow does not appear explicitly. The impedance boundary condition can be directly written $\xi = -p/(\mathrm{i}\omega\rho_0 c_0 Z)$ and $\xi = p/(\mathrm{i}\omega\rho_0 c_0 Z)$ for the lower and upper walls, respectively.

In each section, the pressure p and displacement ξ are both written in modal form, as in Eq. (4). Assuming that p and ξ have an axial dependence given by $\mathrm{e}^{-\mathrm{i}k_x x}$ yields

$$\frac{\partial p}{\partial y} - \rho_0(\omega - u_0 k_x)^2\xi = 0, \tag{7a}$$

$$-\rho_0 c_0^2(\omega - u_0 k_x)^2\frac{\partial \xi}{\partial y} + c_0^2 k_x^2 p - (\omega - u_0 k_x)^2 p = 0. \tag{7b}$$

This eigenvalue problem for the axial wavenumbers and mode shape functions is also solved using a pseudo-spectral method, with N Chebyshev polynomials to represent p and ξ. The two equations Eq. (7a) and (7b) are written at $N-1$ Chebyshev collocation points. The linear system is closed by the two boundary conditions.

The sound field in the whole duct is calculated via the same mode-matching method as above [19].

2.2. Calculation of impedance from wavenumbers

A key step in the direct eduction of impedance is to calculate the liner impedance using a measured axial wavenumber. This section describes two methods for this purpose: the classical method assuming that the mean flow is uniform, and a second method

including the effect of a parallel sheared mean flow. These methods can be applied for either a single incident mode case or an incident multimodal field. Two liner configurations are considered for both methods: the 'single-liner configuration' where only the lower duct wall is lined, and the 'double-liner configuration' where both the lower and upper wall are lined by the same material.

2.2.1. Uniform flow

With uniform flow, the mode shape functions that satisfy Eq. (1) can be directly written as

$$\Psi_n(y) = A_n \cos(k_{yn} y) + B_n \sin(k_{yn} y), \tag{8}$$

where the transverse wavenumbers k_{yn} are given by the dispersion relation:

$$k_{yn} = \sqrt{(k_0 - M k_{xn})^2 - k_{xn}^2}, \tag{9}$$

with $M = u_0/c_0$ the mean flow Mach number.

We first consider the single liner configuration where only the lower duct wall is treated. Substituting the above expression for Ψ_n into the Ingard–Myers condition Eq. (3) at $y = 0$ and into the rigid-wall condition Eq. (2) at $y = H$ yields a closed-form expression for the specific impedance Z in terms of the mode wavenumbers [7]:

$$Z = \frac{\mathrm{i}(k_0 - M k_{xn})^2}{k_0 k_{yn} \tan(k_{yn} H)}, \tag{10}$$

where $k_0 = \omega/c_0$ is the free-field wavenumber.

For the double liner configuration, the Ingard–Myers condition Eq. (2) is applied at both the upper and lower walls, with the assumption that they have the same impedance.

This yields the following quadratic equation:

$$R^2 - 2Rk_{yn}\cot(k_{yn} H) - k_{yn}^2 = 0\,, \quad \text{with } R = \frac{(k_0 - M k_x)^2}{\mathrm{i} k_0 Z}\,. \tag{11}$$

The solutions for the impedance are

$$Z = \frac{(k_0 - M k_{xn})^2 \sin(k_{yn} H)}{\mathrm{i} k_0 k_{yn} [\cos(k_{yn} H) \pm 1]}. \tag{12}$$

This expression contains two types of solutions distinguished by "±" in the denominator, in which "−" corresponds to symmetric modes and "+" to antisymmetric modes. The choice is completely controlled by the (anti)symmetry of the incident mode. When the upper and lower walls are lined with the same material, the total sound field will retain the symmetry of the incident mode. For instance, if the incident mode is antisymmetric, then one should use the sign "+" in the expression above.

Spillere et al. also provide an expression to calculate the impedance for both configurations, see Eq. (7) in [3]. However, their expression for the double-liner configuration is only applicable to symmetric acoustic fields. The present result in Eq. (12) is equally applicable to both types of incident modes.

2.2.2. Shear flow

With shear flow, it is not possible to write a closed-form expression for the wall impedance like Eq. (10). Instead, the relation between Z and the axial wavenumber k_x remains implicitly defined by the governing equations Eq. (7). To compute the impedance Z associated to a given k_x, one approach is to use a non-linear optimisation method to iteratively adjust Z until one of the duct modes in the lined section has the expected wavenumber k_x. This approach requires solving the model presented in Section 2.1.2 many times, which can be costly [4]. Here, we reuse and extend the method from [14] to compute the wall impedance in a single calculation. In contrast with Section 2.1.2, Eq. (7) are now solved only in the lined section, for a known k_x and with modified boundary conditions.

For the case of a single liner on the lower wall $y = 0$, two boundary conditions are imposed on the hard wall (at $y = H$), while no condition is imposed on the lined wall. More specifically, the normal displacement is set to zero on the upper wall, $\xi(y = H) = 0$, which is consistent with a rigid surface, and pressure is also prescribed on that wall: $p(y = H) = 1$. These boundary conditions are sufficient to obtain a well-posed differential equation. This model is solved numerically with the same pseudo-spectral method as in Section 2.1.2. It is then straightforward to compute the impedance of the lined wall at $y = 0$:

$$Z = \frac{-p(0)}{\mathrm{i}\omega\rho_0 c_0 \xi(0)}. \tag{13}$$

This expression shows that the value of Z is independent of the amplitude of the sound field. This justifies the fact that $p(H)$ can be set to any non-zero value.

The procedure has to be modified for the case where the two walls are lined with the same impedance. Two separate solutions are computed. The solutions $p_1(y)$ and $\xi_1(y)$ satisfy $p_1(H) = 1$ and $\xi_1(H) = 0$, while the solutions $p_2(y)$ and $\xi_2(y)$ satisfy $p_2(H) = 0$ and $\xi_2(H) = 1$. We then construct a linear combination of these solutions:

$$\begin{aligned} p(y) &= c_1 p_1(y) + c_2 p_2(y), \\ \xi(y) &= c_1 \xi_1(y) + c_2 \xi_2(y), \end{aligned}$$

so that this new solution has the same impedance at the two walls. In other words, we seek the constants c_1 and c_2 such that

$$\rho_0 c_0 Z = \frac{p(H)}{\mathrm{i}\omega\xi(H)} = \frac{p(0)}{-\mathrm{i}\omega\xi(0)}. \tag{15}$$

This expression reduces to a quadratic equation for Z:

$$\omega^2\rho_0^2 c_0^2 \xi_1(0) Z^2 - i\omega\rho_0 c_0[\xi_2(0) + p_1(0)]Z - p_2(0) = 0\ . \tag{16}$$

One of the two roots corresponds to a symmetric solution, while the other corresponds to an antisymmetric solution. Using the same argument as in Section 2.2.1, it is easy to identify the correct value of Z based on the (anti)symmetry of the incident duct mode.

3. Parametric study on shear flow effects

This section considers two aspects: the influence of the mean flow shear on the acoustic propagation, in terms of the acoustic mode wavenumbers, and the validity of the uniform flow assumption used when calculating the wall impedance from the knowledge of an acoustic axial wavenumber.

The parametric studies are presented using non-dimensional parameters and results, based on the reference values ρ_0, c_0 and H. For instance, the angular frequency ω is converted into the Helmholtz number $He = \omega H/c_0$. This Helmholtz number will vary between 0.1 and 16, which covers a wide range of experimental facilities. For instance, for a small duct facility ($H = 4$ cm in [20]) operating between 300 and 3000 Hz, the Helmholtz number varies roughly between 0.22 and 2.2. In contrast, for a large duct facility ($H = 28$ cm in [21]) operating in the same frequency range, He varies between 1.6 and 15.5 approximately.

A constant value $Z = 1 - \mathrm{i}$ is used for the liner impedance. Other choices have been used by the authors, including frequency dependent impedance functions, and the conclusions remain the same.

3.1. Effects on the acoustic propagation

We begin with the influence of the mean flow shear on the acoustic propagation, which is assessed as changes in the duct mode wavenumbers. These wavenumbers are calculated here for uniform flows and for shear flows using the methods introduced in Sections 2.1.1 and 2.1.2. The velocity profile of the shear flow uses an inverse power law:

$$\frac{u_0(y)}{u_{0\max}} = \begin{cases} (y/\delta)^{1/n}, & 0 \le y \le \delta, \\ 1, & \delta \le y \le 1-\delta, \\ [(1-y)/\delta]^{1/n}, & 1-\delta \le y \le 1, \end{cases} \tag{17}$$

where we have introduced the boundary layer thickness δ, the power n and the maximum velocity $u_{0\max}$. To study the effect of the boundary layer on sound propagation, it is recommended to use the displacement boundary layer thickness δ_1 to characterise the boundary layer [22]. For the profile defined above, we have $\delta_1 = \delta/(n+1)$. The present parametric study will therefore focus on varying δ_1 instead of δ. Instead of defining directly the order n of the power law, we use the shape factor θ, which is the ratio of the displacement thickness to the momentum thickness of the boundary layer (for the profile Eq. (17) we have $\theta = 1 + 2/n$). The shape factor is fixed to $\theta = 1.55$ which is typical of turbulent boundary layers. When comparing results between the uniform flow and the shear flow, we will use the same average Mach number M_{ave} for the two cases.

The velocity profile given in Eq. (17) presents discontinuities of the velocity gradient at $y = \delta$ and $1-\delta$. This can be detrimental to the accuracy of the spectral method used here. A simple way to mitigate this is to smooth the profile by introducing blending functions that quickly but smoothly transition from one part of the profile to the next. Appendix gives the detailed definitions of these blending functions. This smoothing has a negligible effect on the flow properties δ_1, θ and M_{ave}.

3.1.1. Boundary layer thickness

The displacement thickness δ_1 is varied between 0.01 and 0.1, corresponding to 1% and 10% of the duct height, respectively. This range of values is based on various velocity profile measurements on several facilities with different duct heights and Mach numbers. The mean flow velocity is $M_{\mathrm{ave}} = \pm 0.3$, with the sign + (resp. −) corresponding to the acoustic mode propagating downstream with the flow (resp. upstream against the flow). The velocity profiles are shown in Fig. 2.

Fig. 3 shows the axial wavenumbers $k_{x,\mathrm{u}}$ and $k_{x,\mathrm{s}}$ calculated respectively for the uniform flow and the shear flow with various boundary layer thicknesses in the single liner case. Only the first mode k_{x1} corresponding to the plane wave in the hard-wall duct is included, but the same conclusions can be drawn for the other modes. The linear scaling of the axial wavenumber with the frequency is clearly visible. The variation of the wavenumber with δ_1 are visible for the imaginary part but difficult to assess for the real part.

It is therefore preferable to plot the differences between wavenumbers $k_{x,\mathrm{s}} - k_{x,\mathrm{u}}$ to investigate the shear flow effects, as shown in Fig. 4. Overall, the differences between uniform and sheared flows increase systematically with the boundary layer thickness δ_1. For downstream propagation and with a single liner, see Fig. 4(a), there is little difference between the uniform and shear flow cases when $He \lesssim 5$. For higher frequencies, one can observe that $k_{x,\mathrm{s}}$ diverge more significantly from $k_{x,\mathrm{u}}$. For upstream propagation, shown in Fig. 4(b), the differences on the real part of the wavenumber are larger, but the difference on the imaginary part are much smaller and even tend to decrease at higher frequencies.

For the double liner configuration, the trend observed in Fig. 4(c) is similar to the single liner case, with an increased difference at higher frequencies ($He \gtrsim 6$).

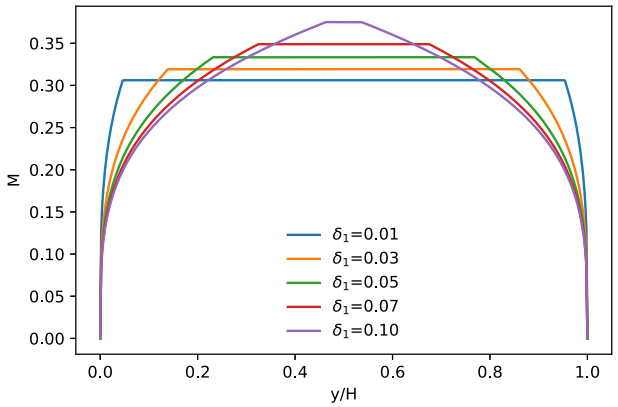

Fig. 2. Examples of velocity profiles in Eq. (17) for different displacement thicknesses, with $M_{\text{ave}} = 0.3$ and $\theta = 1.55$.

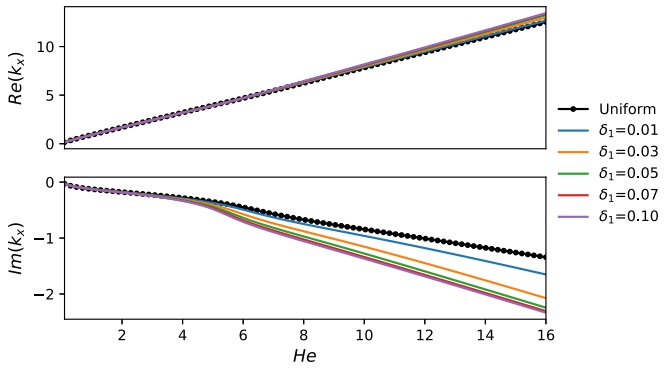

Fig. 3. Axial wavenumbers k_{x1} calculated with the uniform flow or with the shear flow with different displacement thicknesses (flow velocity: $M_{\text{ave}} = +0.3$) for the single liner configuration.

Fig. 4(d) shows that the differences for upstream propagation and a double liner are also similar to the single liner cases, but with increased differences at low frequencies.

The main trends to note in these results is that, as expected, the effect of the boundary layer is more significant for larger δ_1 and for upstream sound propagation at high frequencies. For experimental facilities with small duct ($He \lesssim 5$), the mean flow shear can be largely ignored, except for upstream propagation with a double liner. For facilities with larger ducts ($He \gtrsim 5$), the sheared mean flow should be taken into account.

3.1.2. Mean flow velocity

To assess the influence of the flow velocity, we vary M_{ave} between 0.1 to 0.7 in both directions. The boundary layer thickness δ_1 is set to 0.05, which is a typical value measured in experiments.

In Fig. 5, the differences in wavenumbers $k_{x,\text{s}} - k_{x,\text{u}}$ follow a similar trend with both the single and double liners. For downstream propagation ($M_{\text{ave}} > 0$), shown in Fig. 5(a) and 5(c), the differences remain small when $He \lesssim 5$, similar to the previous section. However, the differences become significant for larger frequencies, and the increase in the mean flow velocity only impacts slightly the magnitude of the wavenumber differences. For upstream propagation ($M_{\text{ave}} < 0$), as shown in Fig. 5(b) and 5(d), the differences are much larger, even for low frequencies. In this case, there is a clear trend whereby increasing the mean flow velocity increases the differences in wavenumber.

To summarise, for downstream propagation, the mean flow shear has little influence on the acoustic propagation in small ducts and a more visible influence in larger ducts. However, the effect of mean flow shear is much more important for upstream propagation (including in small duct) and even more so for the double liner configuration.

3.2. Accuracy of the impedance calculation

We now discuss the validity of the uniform flow assumption traditionally used when calculating the liner impedance given a set of wavenumbers. The parametric study still focuses on the influence of the boundary layer thickness and the flow velocity, which vary in the same range as previously. The duct mode wavenumbers $k_{x,s}$ are first calculated in the lined section using the shear flow

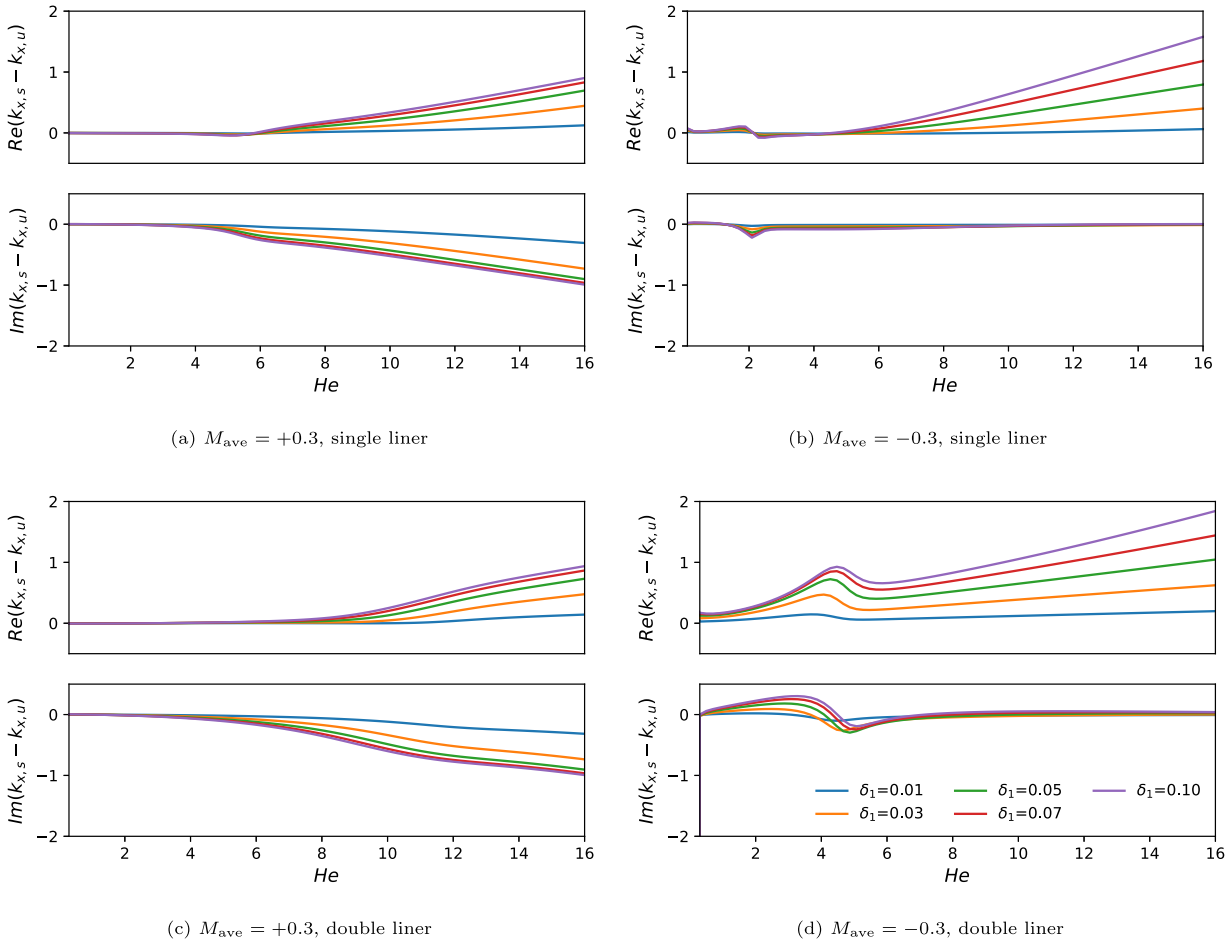

(a) $M_{\text{ave}} = +0.3$, single liner

(b) $M_{\text{ave}} = -0.3$, single liner

(c) $M_{\text{ave}} = +0.3$, double liner

(d) $M_{\text{ave}} = -0.3$, double liner

Fig. 4. Differences between axial wavenumbers $k_{x,s} - k_{x,u}$ obtained with a uniform or sheared flow as a function of the Helmholtz number He. (a,b): single liner configuration. (c,d): double liner configuration.

model from Section 2.1.2. These wavenumbers are then used as input for the two methods presented in Section 2.2 to calculate the impedance, either for a single liner or a double liner. The analysis compares the imposed value of the liner impedance and the calculated results Z_u or Z_s, where Z_u is the impedance obtained under the assumption of a uniform flow (Section 2.2.1), while Z_s is computed by the shear flow method (Section 2.2.2).

3.2.1. Boundary layer thickness

Fig. 6 displays the difference between the calculated impedance and the imposed value, either for the uniform flow model or the shear flow model. The Mach number is $M_{\text{ave}} = \pm 0.3$, and the displacement thickness δ_1 varies between 0.01 and 0.1.

The dashed lines in Fig. 6 show that, in all cases, there is no error on the calculated impedance when using the shear flow model from Section 2.2.2. This is to be expected since the same propagation model with shear flow Eq. (7) is used to calculate the axial wavenumber in the first place, and then to recover the impedance.

More interesting in Fig. 6 is the quantitative assessment of the error introduced by assuming a uniform mean flow when calculating the impedance. As expected, the error on the impedance is steadily growing as we increase the boundary layer thickness. For Helmholtz numbers smaller than 3 or 4, the error on Z can be considered negligible. For downstream propagation and frequencies $He \gtrsim 5$ the error is larger, but the calculated impedance remains within 0.4 from the imposed value. However, for frequencies $He \gtrsim 5$, the discrepancies are much more important for upstream propagation (at least an order of magnitude larger). This indicates that the uniform flow assumption is only valid for small ducts and low frequencies. For large ducts, it is important to include the effect of the mean flow shear when waves are propagating upstream.

3.2.2. Mean flow velocity

To assess the effect of the mean flow velocity on the impedance calculation, Fig. 7 shows the error in the calculated impedance as a function of the average Mach number M_{ave}. Since the results are very similar in both liner configurations, only the single liner results are presented for brevity.

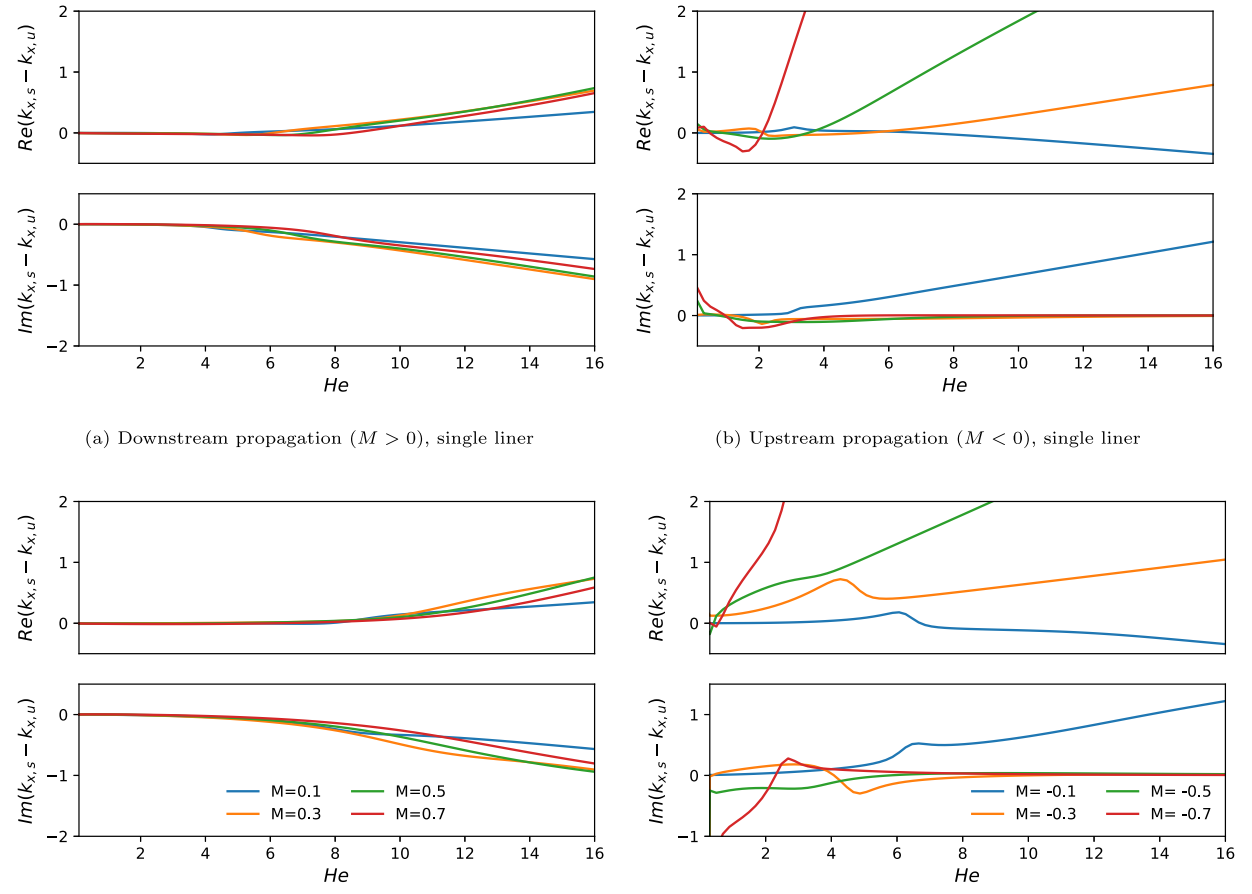

(a) Downstream propagation ($M > 0$), single liner

(b) Upstream propagation ($M < 0$), single liner

(c) Downstream propagation ($M > 0$), double liner

(d) Upstream propagation ($M < 0$), double liner

Fig. 5. Differences between axial wavenumbers $k_{x,s} - k_{x,u}$ obtained with a uniform and sheared flow as a function of the Helmholtz number He. The mean Mach number M_{ave} is varied between 0.1 and 0.7 for both directions. (a,b): single liner configuration. (c,d): double liner configuration.

Again, the results calculated using the shear flow method are in perfect agreement with the imposed value, as expected. For the results calculated using the uniform flow assumption, the discrepancies with the imposed value tend to increase with the mean flow Mach number. For downstream propagation at low frequencies, these discrepancies can still be considered negligible. But the error increases steadily for higher frequencies to reach approximately 0.5. The situation is much worse for upstream propagation, where the error on the impedance is significantly larger at all frequencies (with the exception of the smallest flow velocity $M_{ave} = -0.1$ for which the error remains small at all frequencies).

The same conclusions as in the previous section can be drawn. For small ducts and low frequencies, the effect of the mean flow shear can be safely neglected. For large ducts or high frequencies, the uniform flow assumption is inaccurate, especially for upstream propagation. It is therefore recommended to use the shear flow method from Section 2.2.2 for accurate calculation of the wall impedance based on the axial wavenumber.

4. Simulated impedance eduction

In the last part of this paper, we use numerical calculations to simulate the experimental process of direct impedance eduction. This method uses a linear microphone array installed in the lined section of the duct, either facing the liner [13] or on the lateral wall of the duct [8]. The pressure signals from the microphones are post-processed to estimate the axial wavenumbers that compose the sound field, from which the effective impedance of the liner can be calculated with the methods proposed in Section 2.2.

4.1. Numerical experiments

4.1.1. Setup

To simulate a representative experimental setup, we use the parameters of the MAINE Flow facility introduced in [21] and modelled here as a 2D duct. The considered configuration is comparable to the one depicted in Fig. 1 where the duct height is

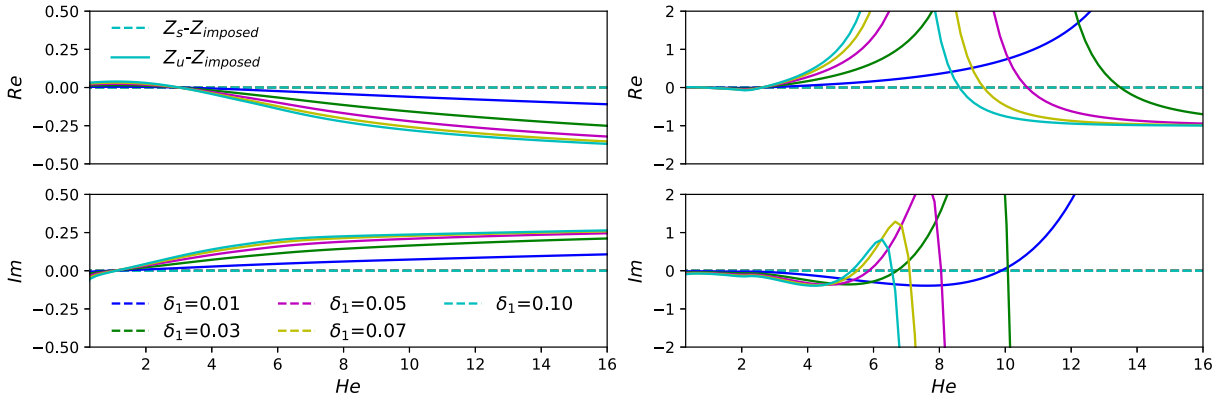

(a) $M_{\text{ave}} = +0.3$, single liner (b) $M_{\text{ave}} = -0.3$, single liner

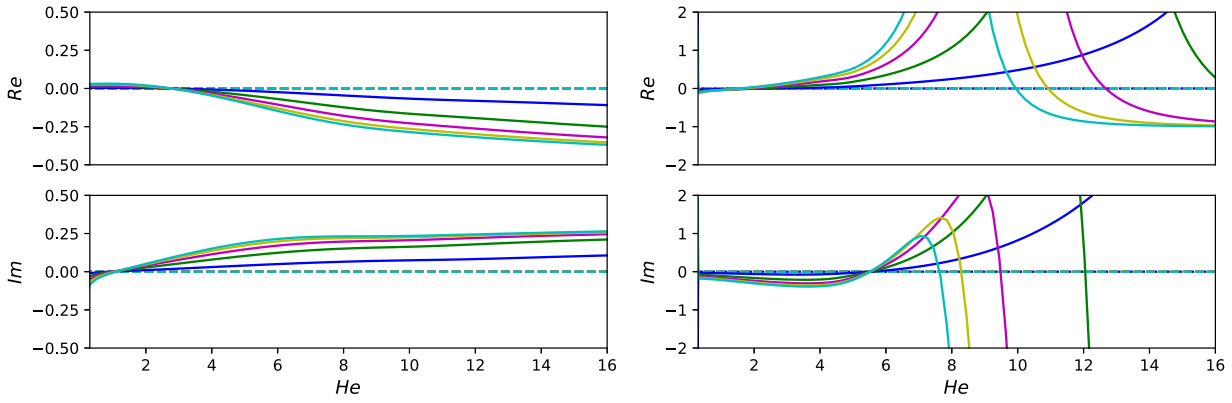

(c) $M_{\text{ave}} = +0.3$, double liner (d) $M_{\text{ave}} = -0.3$, double liner

Fig. 6. Differences between the calculated impedance and the imposed impedance $Z_u - Z_{imposed}$ (solid lines) and $Z_s - Z_{imposed}$ (dashed lines). With δ_1 varying from 0.01 to 0.1 and $M_{ave} = \pm 0.3$. (The y-axis range is adjusted for the visibility of difference.).

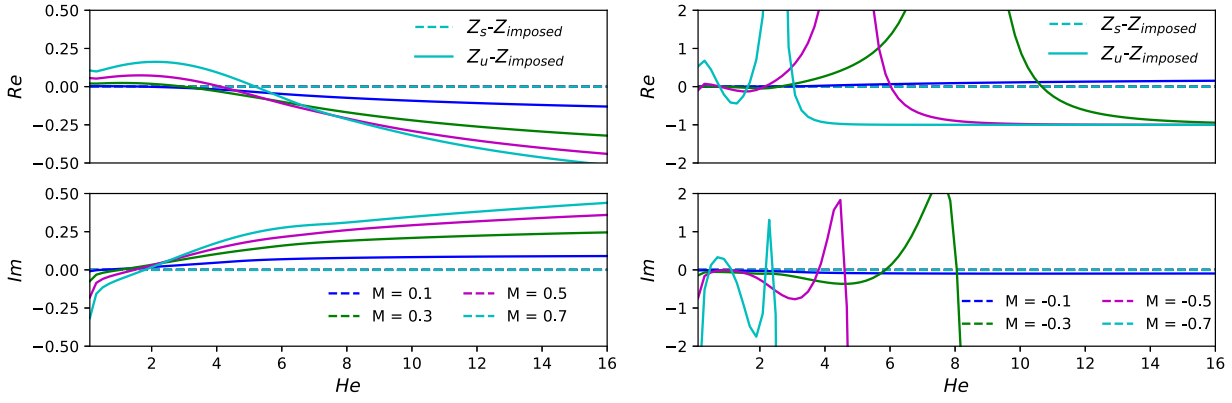

(a) $M = +0.3$, single liner (b) $M = -0.3$, single liner

Fig. 7. Differences between the calculated impedance and the imposed impedance $Z_u - Z_{imposed}$ (solid lines) and $Z_s - Z_{imposed}$ (dashed lines). With M_{ave} varying from 0.1 to 0.7 in both directions, $\delta_1 = 0.05$.

0.28 m, the width is 0.15 m, and the lined section has a length of 0.8 m. The linear microphone array consists of 40 microphones separated by a distance $\Delta x = 0.02$ m where the first and last microphones are placed 0.01 m into the lined section. When only one

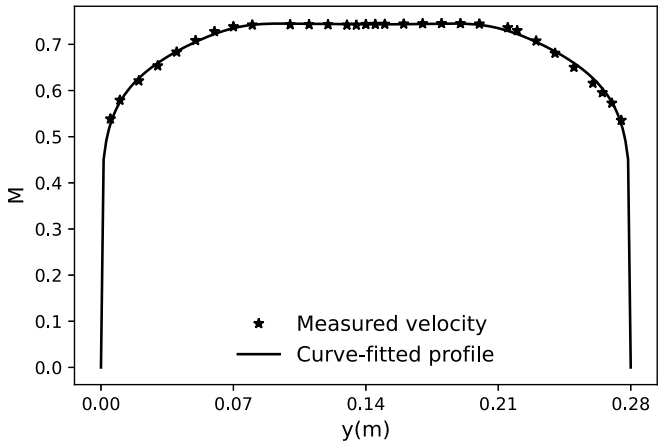

Fig. 8. Measured and fitted mean velocity profile in the cross-section of the MAINE Flow facility. The fitted profile is obtained using Eq. (17).

wall is lined, the microphone array is located at 2/3 of the duct height, following the configuration proposed by NASA [8]. For the double liner configuration, and in order to increase our chances for a robust eduction by improving the signal to noise ratio, the vertical position of the microphone line is changed depending on the incident acoustic mode. For antisymmetric modes, the array is still located at 2/3 of the duct height in order to avoid pressure zeros. However, for the case of a symmetric incident mode, the microphone array is placed at the half of the duct height, where the pressure is maximum.

In the following, the liner is a Single Degree of Freedom (SDOF) liner with a specific impedance given by $Z(\omega) = 1 - \mathrm{i}\cot(k_0 h_{\mathrm{cav}})$. The first term models a perforated facing sheet with a constant resistance while the second term represents the acoustic reactance of a cavity of depth $h_{\mathrm{cav}} = 0.03\,\mathrm{m}$. Given this boundary condition, the acoustic field is computed between 300 and 3000 Hz using the numerical method with shear flow described in Section 2.1.2. The mean flow velocity profile is obtained by fitting the inverse-power law profile in Eq. (17) to data measured using a Pitot tube at the mid-width in the cross–section of MAINE Flow [21]. Fig. 8 shows the corresponding data points and the fitted velocity profile.

4.1.2. Wavenumber estimation

In the direct eduction method, the pressure field measured along the microphone array is represented as a sum of exponentials containing modal amplitudes and axial wavenumbers. The latter are determined using a HTLS technique (Harmonic retrieval via Total Least Squares) [23].

This method exploits the shift-invariance property of the Hankel matrix of the signals, together with its singular value decomposition (SVD). Each of the L rows of the Hankel matrix $\mathbf{H}$ contains R pressure values from the microphone array:

$$\mathbf{H} = \begin{pmatrix} p(1) & p(2) & \cdots & p(R) \\ p(2) & p(3) & \cdots & p(R+1) \\ \vdots & \vdots & \ddots & \vdots \\ p(L) & p(L+1) & \cdots & p(N) \end{pmatrix}, \tag{18}$$

where N is the total number of microphones. The integers L and R are chosen so that $N = L + R - 1$. To obtain reliable results, it is recommended in Ref. [24] that L should be between 40% and 60% of N. Thus, in our case with 40 microphones, L is set to 22.

An SVD of the Hankel matrix $\mathbf{H}$ yields the matrix $\mathbf{U}$ of left singular vectors. The shift-invariance property of $\mathbf{U}$ can be written $\mathbf{U}_{\uparrow} \approx \mathbf{U}_{\downarrow}\mathbf{Q}$ with $\mathbf{Q} = \mathrm{diag}\{q_1, q_2, \ldots, q_K\}$. The matrices $\mathbf{U}_{\uparrow}$ and $\mathbf{U}_{\downarrow}$ represent the matrix $\mathbf{U}$ with its top or bottom row removed. The next step is to perform an SVD of the block matrix $[\mathbf{U}_{\downarrow}\, \mathbf{U}_{\uparrow}]$ to obtain its matrix $\mathbf{W}$ of right singular vectors. The matrix $\mathbf{Q}$ can then be estimated by calculating

$$\widetilde{\mathbf{Q}} = -\mathbf{W}_{12}\mathbf{W}_{22}^{-1}, \quad \text{with } \mathbf{W} = \begin{bmatrix} \mathbf{W}_{11} & \mathbf{W}_{12} \\ \mathbf{W}_{21} & \mathbf{W}_{22} \end{bmatrix}, \tag{19}$$

where the rows and columns of $\mathbf{W}$ have been split in half to define the four blocks of $\mathbf{W}$. The coefficients q_k are estimated as the eigenvalues of $\widetilde{\mathbf{Q}}$. Each coefficient q_k is then directly related to an axial wavenumber through the relation $q_k = \exp\{-\mathrm{i}k_{x,k}\Delta x\}$.

Not all the wavenumbers identified by the HTLS technique correspond to physical acoustic modes in the duct lined section. It is therefore necessary to filter out the spurious results and select a physical wavenumber that will be adequate for the impedance eduction. Firstly, we expect the physical wavenumbers k_x to be located in specific regions of the complex plane. For acoustic modes propagating in the positive axial direction in a hard-walled duct with uniform flow, their axial wavenumbers are located in a quadrant of the complex plane defined by

$$\mathrm{Im}(k_x) \le 0\,, \quad \mathrm{Re}(k_x) \ge k_0 \frac{M_{\mathrm{ave}}}{M_{\mathrm{ave}}^2 - 1}\,.$$

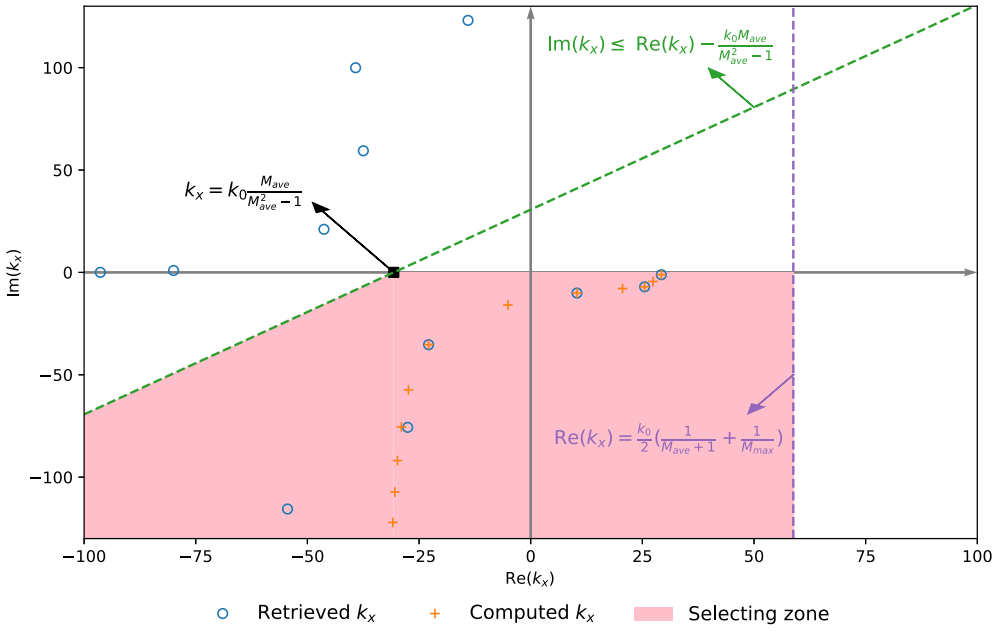

Fig. 9. Illustration of the computed and retrieved wavenumbers in orange plus signs and blue circles, respectively, and the pink region to select the wavenumbers used in the subsequent impedance eduction. The green dashed line stands for Eq. (20); the purple dashed line for Eq. (21). The case is: the double liner configuration, incident plane mode, $M_{ave} = 0.5$ and $f = 2500$ Hz. (For interpretation of the references to colour in this figure legend, the reader is referred to the web version of this article.)

For a lined duct with a parallel sheared flow, this criterion only gives a qualitative indication as to the nature of a wavenumber. To identify right-running modes, the following heuristic rule is used

$$\mathrm{Im}(k_x) \leq \mathrm{Re}(k_x) - k_0 \frac{M_{\mathrm{ave}}}{M_{\mathrm{ave}}^2 - 1} \,. \tag{20}$$

This corresponds to the region of the complex plane below the diagonal intersecting with the real axis at $k_x = k_0 M_{\mathrm{ave}}/(M_{\mathrm{ave}}^2 - 1)$. With a uniform flow with Mach number M_{ave}, this is the wavenumber of modes that are just cut-on. Moreover, only modes on or below the real axis are used, so as to exclude unphysical modes with positive attenuation rates.

Secondly, when $M_{\mathrm{ave}} > 0$ the above condition does not separate acoustic modes from hydrodynamic modes, and a second criterion is needed. For acoustic modes, the largest expected value for $\mathrm{Re}(k_x)$ is close to $k_0/(1+M_{\mathrm{ave}})$. For hydrodynamic modes when $M_{\mathrm{ave}} > 0$, the smallest value of $\mathrm{Re}(k_x)$ is expected to be close to k_0/M_{max} with M_{max} being the largest Mach number of the velocity profile. We therefore use the average of these two values as a threshold to discriminate between acoustic and hydrodynamic modes. More specifically, a wavenumber is retained as an acoustic mode if

$$\mathrm{Re}(k_x) < \frac{k_0}{2}\left(\frac{1}{M_{\mathrm{ave}}+1} + \frac{1}{M_{\mathrm{max}}}\right) \,. \tag{21}$$

The conditions Eqs. (20) and (21) are only qualitative, but their robustness has been proven in practice. For example, Fig. 9 shows the region defined to select the retrieved wavenumbers in the double-liner configuration with an incident plane wave at $f = 2500$ Hz and with $M_{\mathrm{ave}} = 0.5$. The wavenumbers computed numerically are also shown to compare with those retrieved by the HTLS method.

After enforcing these conditions, several of the wavenumbers calculated by the HTLS technique remain, and one of them should be selected for the impedance eduction. In the literature [5,7,17] it is common to use the least attenuated mode for the impedance eduction, i.e. the wavenumber closest to the real axis. This choice is well suited for small ducts and at low frequencies (that is, for small Helmholtz numbers) where only the plane wave is propagating, and the sound field is composed of a single mode in each direction. For large ducts or at high frequencies, it is possible to have several modes that are only weakly attenuated and the sound field in the lined section is clearly composed of several modes. In such cases, and according to our simulations, the least attenuated wavenumber does not always yield the most accurate result for the impedance eduction.

For this reason, we propose an improved criterion to select the wavenumber, based on the number of cut-on modes in the hard-wall section of the duct. The wavenumbers identified in the lined section are selected using the constraints described above and ordered by their rate of attenuation (i.e. based on the value of $|\mathrm{Im}(k_x)|$). For a given frequency, if n modes are cut-on in the hard-wall duct, the nth wavenumber calculated by the HTLS technique will be used to calculate the liner impedance. For instance, with the single-liner configuration, if two modes are cut-on in the hard-wall section, then the second wavenumber will be used to calculate the impedance. Note that for the double-liner configuration, only the cut-on modes with the same symmetry as the

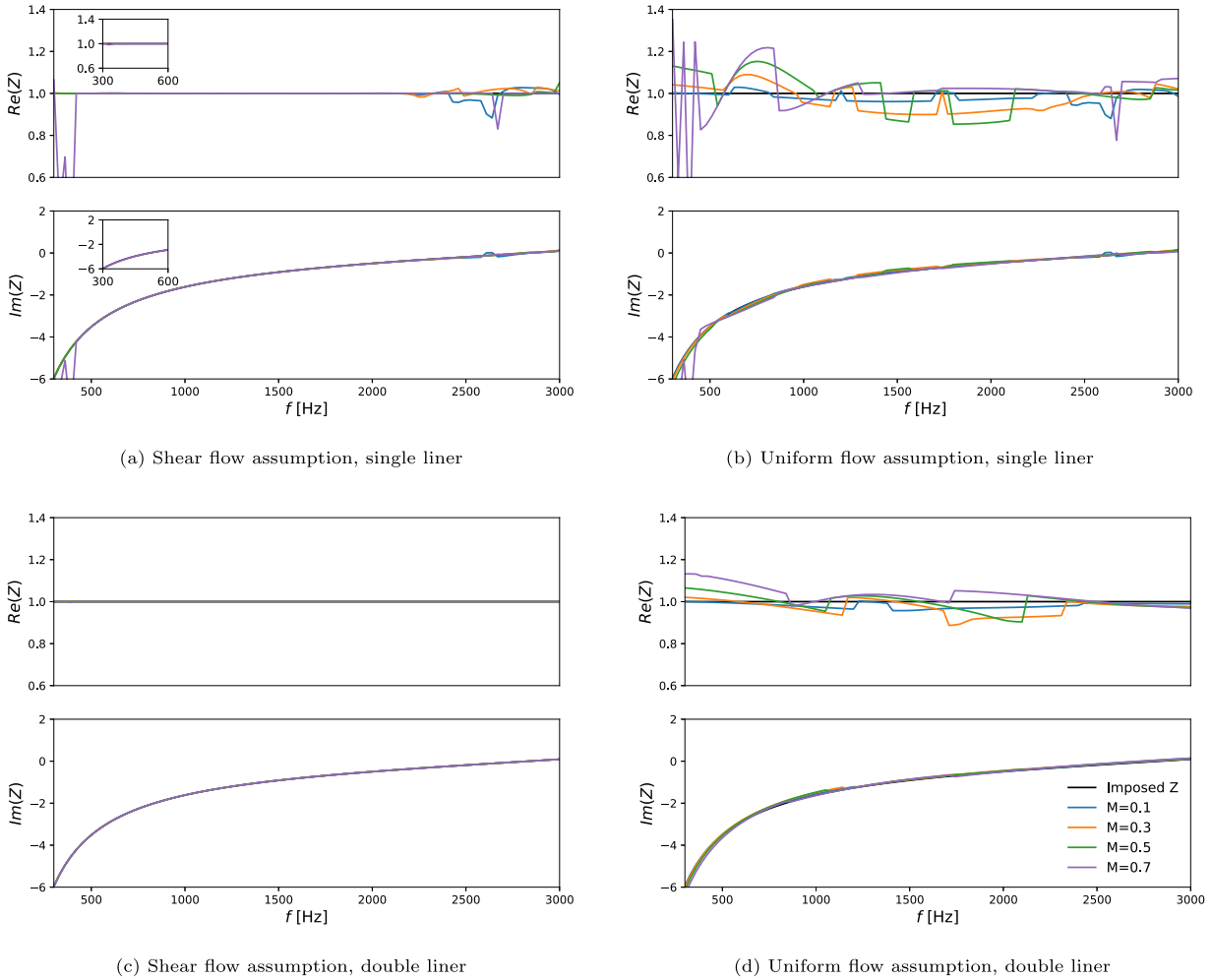

(a) Shear flow assumption, single liner

(b) Uniform flow assumption, single liner

(c) Shear flow assumption, double liner

(d) Uniform flow assumption, double liner

Fig. 10. Educed impedance without noise using the uniform (right) and shear (left) flow assumption, for different flow velocities in the same direction as the incident plane wave. The insets show the impedance calculated using the second educed wavenumber. Top: single-liner configuration. Bottom: double-liner configuration. Black solid line: imposed impedance.

incident wave should be counted. For instance, with the double-liner configuration, if the incident mode is symmetric and there are two symmetric cut-on modes in the hard-wall duct, then the second measured wavenumber will be used. This is because the total sound field retains the symmetry of the incident mode in the double-liner configuration. This property is also visible in the example in Fig. 9 where only symmetric modes are identified by the HTLS technique.

4.1.3. Background noise

The presence of noise in the experiments, produced mainly by the turbulent boundary layer above the microphones, can significantly impact the impedance eduction results. In this study, the background noise is simulated by adding random signals to the simulated pressure signals calculated at the microphone positions. The noise signals are assumed to be uncorrelated between microphones and are generated with an amplitude following a normal distribution with mean value 0 and standard deviation σ. The random phase follows a uniform distribution in the range $[0, 2\pi]$. The Signal-to-Noise Ratio (SNR) is defined as $10\log_{10}[P_i^2/\sigma^2]$, where P_i is the pressure amplitude of the incident mode. In the results presented below, we set $P_i = 1$ and the SNR is readily adjusted by setting σ.

4.2. Results without noise

To validate the proposed eduction configuration, the eduction process is first simulated without noise perturbation. The Mach number is varied from 0.1 to 0.7 by scaling the fitted flow profile already shown in Fig. 8. The supplementary criterion described in Section 4.1.2 is applied.

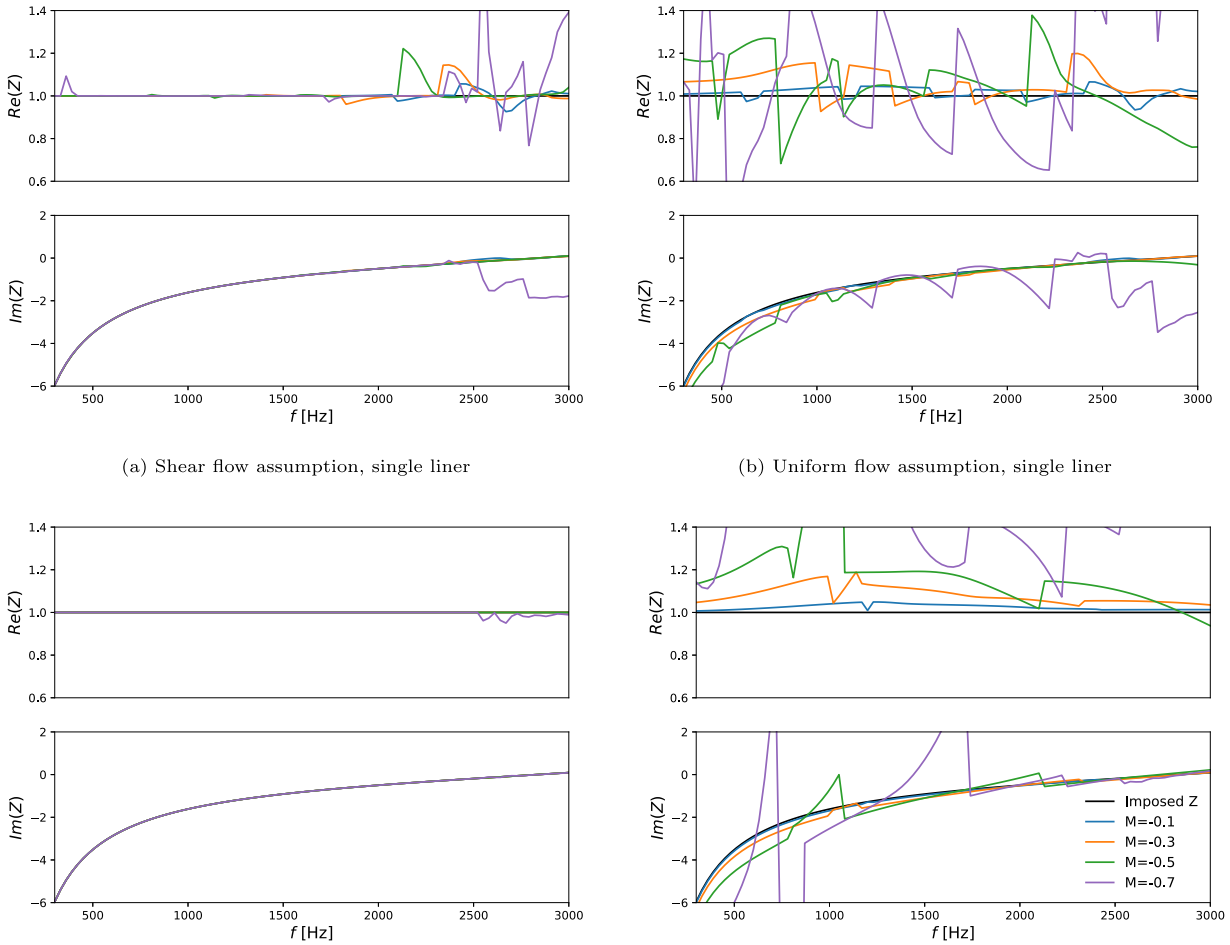

(a) Shear flow assumption, single liner

(b) Uniform flow assumption, single liner

(c) Shear flow assumption, double liner

(d) Uniform flow assumption, double liner

Fig. 11. Educed impedance without noise using the uniform (right) and shear (left) flow assumption, for different flow velocities in the opposite direction as the incident plane wave. Top: single-liner configuration. Bottom: double-liner configuration. Black solid line: imposed impedance.

Fig. 10 compares the educed impedance obtained by assuming a uniform or a sheared mean flow in the impedance calculation, while the pressure was calculated by taking into account shear. The results obtained with the plane wave as the incident mode in the downstream direction and for the single and double liner configurations are shown. The results in Fig. 10(a) and (c), obtained with the shear flow assumption, show an excellent agreement with the imposed impedance for the two liner configurations (except at high frequencies for the single liner configuration). Increasing the flow velocity makes little difference to the agreement of the eduction results, except at low frequencies for $M_{\text{ave}} = 0.7$. In that specific case, results can be improved by selecting the second educed wavenumber, as shown in the inset graphs of Fig. 10. When using the uniform flow assumption, the double liner configuration tends to improve the accuracy of the educed impedance, as seen by comparing Fig. 10(b) with (d). However, the impedance educed with the uniform flow assumption shows notable discrepancies from the imposed value that increase with the flow velocity. This is because the formula in Eq. (12) based on the uniform flow assumption is not able to represent accurately the relationship between axial wavenumbers and wall impedance in large ducts.

Fig. 11 presents the eduction results with the plane mode incident in the upstream direction. The results in Fig. 11(a) and (c), obtained with the shear flow model, show an excellent agreement with the imposed impedance for both liner configurations (except at high frequencies for the single liner configuration). Using the uniform flow assumption with Ingard–Myers boundary condition as done in Fig. 11(b) and (d) leads to very poor agreement when the flow velocity is greater than $M_{\text{ave}} = -0.1$.

The eduction results above demonstrate that using the shear flow model combined with the double liner configuration yields significant benefits compared to the standard approach (that is, the model based on the uniform flow assumption and the single liner configuration). Similar comparisons have also been performed with single incident higher-order modes (not shown here), and the conclusions remain the same as above.

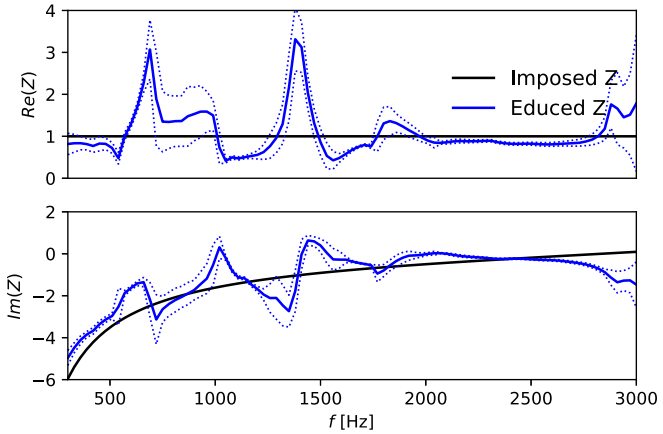

Fig. 12. Educed impedance with noise (SNR = 30 dB) using the shear flow assumption in the single liner configuration. The flow velocity is $M_{\text{ave}} = 0.3$ and the incident plane wave is propagating downstream. Solid line: mean value. Dashed lines: standard deviation.

4.3. Results with noise

We now simulate the eduction process in the presence of noise using a SNR of 30 dB, which is close to what can be observed in the MAINE Flow facility at maximum flow speed. To compute the mean value and the standard deviation of the educed impedance, 1000 realisations of the random noise are calculated, and the eduction process is applied to each one. Note that, in practice, the SNR will vary with frequency, depending on the source strength, the background noise in the test rig and the liner efficiency (e.g. the SNR will decrease when the liner absorption is strong).

As shown in Fig. 12, the eduction results in the single liner configuration exhibit large discrepancies between the imposed and educed impedances at several frequencies below 1800 Hz. This can be explained by the small attenuation of the sound field achieved by a single liner at these frequencies. The small decay of the acoustic pressure over the liner is more easily swamped by the noise added to the microphone data. Fig. 12 shows results obtained with the shear flow assumption. The results obtained with the uniform flow assumption are even worse. For these reasons, only the double liner configuration with the shear flow assumption is presented in the remainder of the study.

Results are shown in Fig. 13 for the educed impedance in the double liner configuration. The first two modes are studied individually, namely mode 0 (plane wave, top panels) and mode 1 (first transverse mode, bottom panels). These are considered representative of the symmetric and antisymmetric modes, respectively. The results for the mode 1 are shown above the cut-on frequency, which varies with the Mach number.

For downstream propagation, in Fig. 13(a), the results with the mode 0 shows a good agreement with the prescribed impedance, and the standard derivation remains acceptable (except close to 800 Hz). In addition, the results obtained for $M_{\text{ave}} = 0.1$ show limited standard derivation, but it becomes larger at higher frequencies. A similar trend is observed for larger Mach numbers M_{ave}.

Comparing Fig. 13(a) and (c) shows that the mean impedance value educed for incident mode 1 is closer to the exact value than for incident mode 0. For $M_{\text{ave}} = 0.5$ and $M_{\text{ave}} = 0.7$, the standard derivation becomes large in the vicinity of the cut-on frequencies used by our criteria, indicating that the noise perturbations are significant. For all the results obtained when waves propagate in the downstream direction, there exists a disparity at high frequencies which might be explained by the appearance of higher-order modes.

In Fig. 13(b) and (d), incident modes propagating in the upstream direction are considered. It is shown that the mean impedance values remain close to the imposed impedance in most of the cases. Note that there is a tradeoff between the number of considered modes and the avoidance of noise perturbations when estimating the wavenumbers. If more wavenumbers are needed, more noise will be involved in the calculation. Therefore, the standard variation becomes notable, and the mean value deviates more from the imposed value near the frequency used to split the frequency range. However, high-speed flows in the opposite direction of the incident acoustic wave pose challenging conditions which require more work to be tackled. In particular, for $M_{ave} = -0.7$ the mean impedance value is only close to the imposed one at low frequencies before deviating dramatically.

Except when $M_{\text{ave}} = -0.7$, comparing the results obtained for the two modes shows that the antisymmetric incident mode provides a better performance in the impedance eduction. This inspires an experimental perspective that would use attenuated high-order modes or antisymmetric modes as incident waves to improve the robustness of the method.

To conclude, and according to the results above, using the shear flow method with the double liner configuration improves the accuracy and the reliability of the eduction process. This is critical for understanding the behaviour of acoustic liner submitted to high speed flows and multimodal acoustic conditions where the uniform flow assumption is not applicable any more.

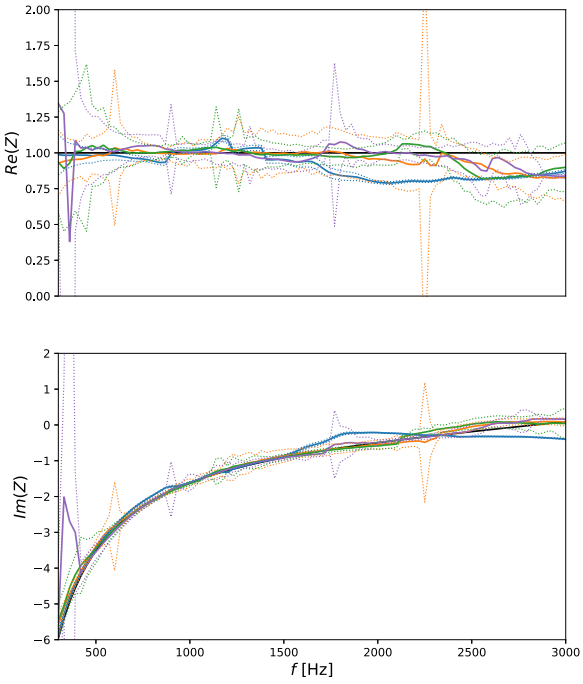

(a) Mode 0, downstream propagation

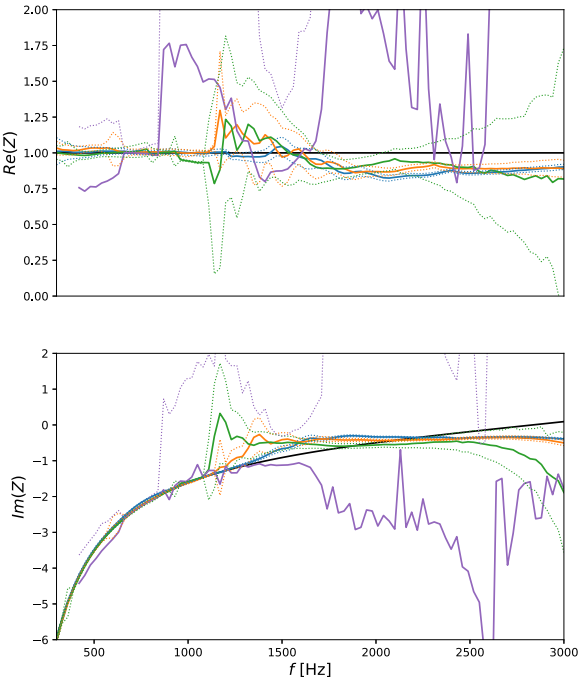

(b) Mode 0, upstream propagation

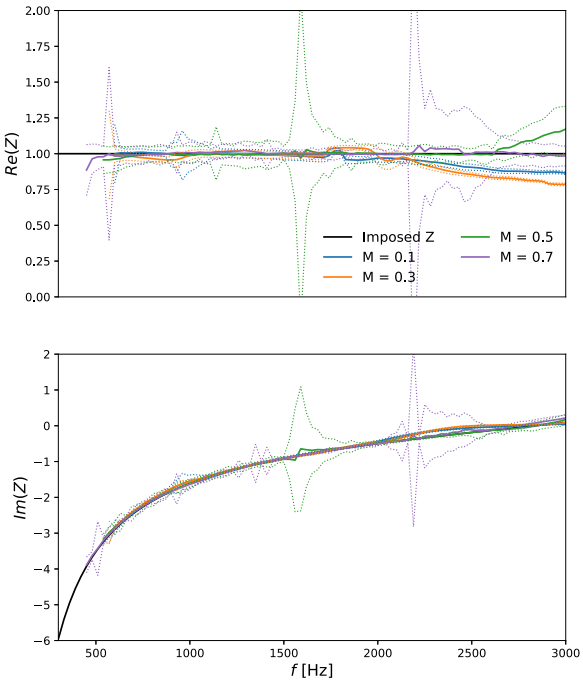

(c) Mode 1, downstream propagation

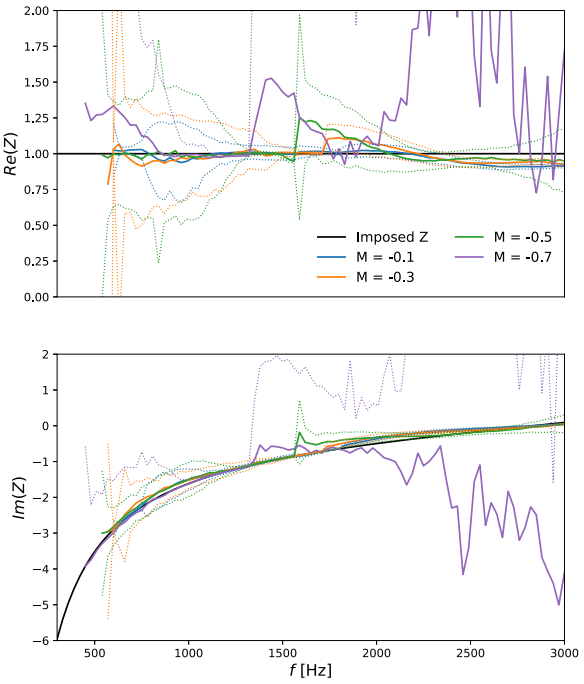

(d) Mode 1, upstream propagation

Fig. 13. Educed impedance with noise (SNR = 30 dB) using the model with sheared flow. Black line: imposed impedance. Coloured solid line: mean value of impedance. Coloured dashed line: standard deviation of the educed impedance around its mean value. (For interpretation of the references to colour in this figure legend, the reader is referred to the web version of this article.)

5. Summary and conclusions

This work assesses the effects of mean flow shear on sound propagation in a 2D duct and on the direct eduction of impedance. The parametric study considers the influence of the Helmholtz number, the displacement boundary layer thickness, the Mach number, the direction of propagation, the liner configuration and the presence of noise. A number of significant results can be noted:

- The influence of the mean flow shear is more important for large Helmholtz numbers. While the uniform mean flow approximation is clearly valid for small ducts at low frequencies, results presented here demonstrate that it is crucial to include the effect of the mean flow shear when considering large ducts and/or high frequencies.
- The shear flow effects are more important for sound propagating upstream, compared to downstream propagation. As expected, the validity of the uniform flow approximation decreases for high flow velocities and thick boundary layers.
- A double liner configuration is proposed, and it is shown to be more robust and less sensitive to the influence of the mean flow shear and to measurement noise, compared to the traditional single-liner configuration. While using two liner samples instead of one increases the cost and complexity of the impedance eduction, the significant benefits in terms of accuracy are likely to justify the additional cost.
- The method proposed in [14] to calculate directly the wall impedance based on the axial wavenumber is generalised to include sound propagation in a parallel shear flow and to consider the double liner configuration.
- For large Helmholtz numbers, there is more than one propagating mode in the hard-wall section of the duct. The use of the plane wave as incident sound field is not always the best option. If one can control the modal content of the incident sound field, it is beneficial to use the higher-order modes. This is likely because these higher-order modes are more attenuated by the liner.
- The criteria to select the axial wavenumber used in the impedance eduction are extended to consider large Helmholtz numbers, where the sound field can include several duct modes of comparable amplitudes.

Future work will include the design and experimental validation of an impedance eduction technique for the large-duct facility MAINE Flow, following the recommendations identified in this work. It would also be interesting to perform a similar parametric study on the flow effects in a 3D lined duct. While the trends identified here will still be relevant, the presence of additional modes and mean flow shear along the depth of the cross section in 3D could bring interesting effects.

CRediT authorship contribution statement

Jinyue Yang: Conceptualization, Formal analysis, Investigation, Methodology, Software, Validation, Writing – original draft, Writing – review & editing. **Thomas Humbert:** Conceptualization, Methodology, Project administration, Supervision, Writing – review & editing. **Joachim Golliard:** Conceptualization, Methodology, Supervision, Writing – review & editing. **Gwénaël Gabard:** Conceptualization, Funding acquisition, Methodology, Project administration, Software, Supervision, Writing – review & editing.

Declaration of competing interest

The authors declare that they have no known competing financial interests or personal relationships that could have appeared to influence the work reported in this paper.

Data availability

Data will be made available on request.

Acknowledgements

The authors acknowledge the financial support of the Safran Group and the Agence Nationale de la Recherche (France) through the Industrial Chair ASTRAL (grant ANR-20-CHIN-00050-01).

Appendix. Smooth velocity profile

The velocity profile is composed of three parts, each using one of the following functions:

$$f_1(y) = u_{0\max}(y/\delta)^{1/n}, \tag{A.1a}$$

$$f_2(y) = u_{0\max}, \tag{A.1b}$$

$$f_3(y) = u_{0\max}[(H-y)/\delta]^{1/n}, \tag{A.1c}$$

where f_1 and f_3 represent the boundary layers and f_2 represents the central region. To construct a smoothly varying profile $u_0(y)$ the three functions defined above are combined with blending functions $b_i(y)$:

$$u_0(y) = \sum_{i=1}^{3} f_i(y)\tilde{b}_i(y)\ . \tag{A.2}$$

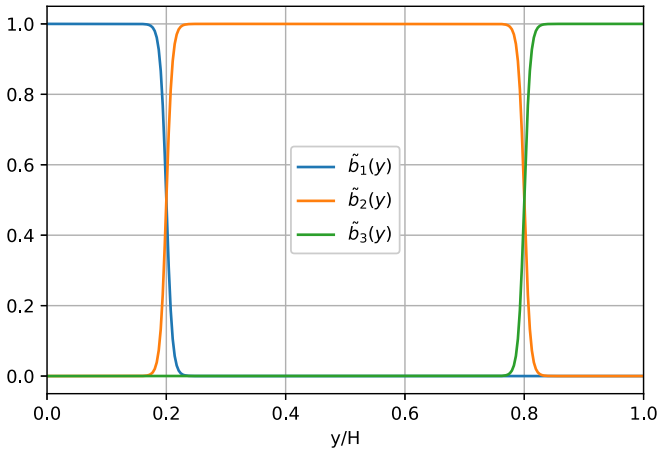

Fig. A.1. Blending functions $\tilde{b}_i(y)$ for $\delta/H = 0.2$ and $d/H = 0.01$.

The blending functions are defined as follows

$$\tilde{b}_i(y) = \left\{ b_i(y) - \min_{0\le y\le H}[b_i(y)] \right\} / \left\{ \max_{0\le y\le H}[b_i(y)] - \min_{0\le y\le H}[b_i(y)] \right\} , \tag{A.3}$$

with

$$b_1(y) = g(\delta - y) , \quad b_2(y) = g(y-\delta)g(H-y-\delta) , \quad b_3(y) = g(y+\delta-H) , \tag{A.4}$$

and

$$g(y) = \frac{1}{2}\left[1 + \tanh\left(\frac{y}{d}\right)\right] . \tag{A.5}$$

The parameter d controls how quickly the functions b_i transition from 0 to 1. The scaling introduced in Eq. (A.3) ensures that the blending functions $\tilde{b}_i(y)$ vary exactly between 0 and 1. With the definition (A.2), the velocity profile $u_0(y)$ and all its derivatives are continuous. An example of blending functions is shown in Fig. A.1 where each blending function can be seen to vary smoothly, and quickly, between 0 and 1 at $y = \delta$ and $y = H - \delta$.

References

[1] Y. Aurégan, M. Leroux, V. Pagneux, Measurement of liner impedance with flow by an inverse method, in: 10th AIAA/CEAS Aeroacoustics Conference, 2004, p. 2838, http://dx.doi.org/10.2514/6.2004-2838.
[2] R. Troian, D. Dragna, C. Bailly, M.-A. Galland, Broadband eduction of liner impedance under multimodal acoustic propagation, in: 22nd AIAA/CEAS Aeroacoustics Conference, 2016, p. 2725, http://dx.doi.org/10.2514/6.2016-2725.
[3] A.M. Spillere, L.A. Bonomo, J.A. Cordioli, E.J. Brambley, Testing impedance eduction boundary conditions with four wavenumbers per frequency, in: 25th AIAA/CEAS Aeroacoustics Conference, 2019, p. 2488, http://dx.doi.org/10.2514/6.2019-2488.
[4] R. Roncen, E. Piot, F. Méry, F. Simon, M.G. Jones, D.M. Nark, Wavenumber-based impedance eduction with a shear grazing flow, AIAA J. 58 (7) (2020) 3040–3050, http://dx.doi.org/10.2514/1.J059100.
[5] W.R. Watson, M.G. Jones, A comparative study of four impedance eduction methodologies using several test liners, in: 19th AIAA/CEAS Aeroacoustics Conference, 2013, p. 2274, http://dx.doi.org/10.2514/6.2013-2274.
[6] C. Weng, A. Schulz, D. Ronneberger, L. Enghardt, F. Bake, Flow and viscous effects on impedance eduction, AIAA J. 56 (3) (2018) 1118–1132, http://dx.doi.org/10.2514/1.J055838.
[7] X. Jing, S. Peng, X. Sun, A straightforward method for wall impedance eduction in a flow duct, J. Acoust. Soc. Am. 124 (1) (2008) 227–234, http://dx.doi.org/10.1121/1.2932256.
[8] W.R. Watson, M.G. Jones, J.C. June, Single mode theory for impedance eduction in large-scale ducts with grazing flow, in: 20th AIAA/CEAS Aeroacoustics Conference, 2014, p. 3351, http://dx.doi.org/10.2514/6.2014-3351.
[9] W.R. Watson, M.G. Jones, Impedance eduction in large ducts containing high-order modes and grazing flow, in: 23rd AIAA/CEAS Aeroacoustics Conference, 2017, p. 3183, http://dx.doi.org/10.2514/6.2017-3183.
[10] L.A. Bonomo, A.M. Spillere, J.A. Cordioli, Parametric uncertainty analysis for impedance eduction based on Prony's method, AIAA J. 58 (8) (2020) 3625–3638, http://dx.doi.org/10.2514/1.J059071.
[11] U. Ingard, Influence of fluid motion past a plane boundary on sound reflection, absorption, and transmission, J. Acoust. Soc. Am. 31 (7) (1959) 1035–1036, http://dx.doi.org/10.1121/1.1907805.
[12] M. Myers, On the acoustic boundary condition in the presence of flow, J. Sound Vib. 71 (3) (1980) 429–434, http://dx.doi.org/10.1016/0022-460X(80)90424-1.
[13] W.R. Watson, M.H. Carpenter, M.G. Jones, Performance of kumaresan and tufts algorithm in liner impedance eduction with flow, AIAA J. 53 (4) (2015) 1091–1102, http://dx.doi.org/10.2514/1.J053705.
[14] X. Jing, S. Peng, L. Wang, X. Sun, Investigation of straightforward impedance eduction in the presence of shear flow, J. Sound Vib. 335 (2015) 89–104, http://dx.doi.org/10.1016/j.jsv.2014.08.031.

[15] M. Jones, W. Watson, D. Nark, Effects of flow profile on educed acoustic liner impedance, in: 16th AIAA/CEAS Aeroacoustics Conference, 2010, p. 3763, http://dx.doi.org/10.2514/6.2010-3763.
[16] R. Roncen, F. Méry, E. Piot, Bayesian inference for modal identification in ducts with a shear flow, J. Acoust. Soc. Am. 146 (4) (2019) 2645–2654, http://dx.doi.org/10.1121/1.5130195.
[17] A. Spillere, J.A. Cordioli, H. Bodén, On the effect of boundary conditions on impedance eduction results, in: 23rd AIAA/CEAS Aeroacoustics Conference, 2017, p. 3185, http://dx.doi.org/10.2514/6.2017-3185.
[18] J.P. Boyd, Chebyshev and Fourier Spectral Methods, second ed., rev, Springer Berlin Heidelberg, Mineola, N.Y, 1989.
[19] G. Gabard, R. Astley, A computational mode-matching approach for sound propagation in three-dimensional ducts with flow, J. Sound Vib. 315 (4–5) (2008) 1103–1124, http://dx.doi.org/10.1016/j.jsv.2008.02.015.
[20] M. D'Elia, T. Humbert, Y. Aurégan, Effect of flow on an array of Helmholtz resonators: Is Kevlar a "magic layer"? J. Acoust. Soc. Am. 148 (6) (2020) 3392–3396, http://dx.doi.org/10.1121/10.0002642.
[21] T. Humbert, J. Golliard, E. Portier, G. Gabard, Y. Auregan, Multimodal characterisation of acoustic liners using the MAINE flow facility, in: 28th AIAA/CEAS Aeroacoustics 2022 Conference, 2022, p. 3082, http://dx.doi.org/10.2514/6.2022-3082.
[22] G. Gabard, Boundary layer effects on liners for aircraft engines, J. Sound Vib. 381 (2016) 30–47, http://dx.doi.org/10.1016/j.jsv.2016.06.032.
[23] J.-M. Papy, L. De Lathauwer, S. Van Huffel, Common pole estimation in multi-channel exponential data modeling, Signal Process. 86 (4) (2006) 846–858, http://dx.doi.org/10.1016/j.sigpro.2005.07.015.
[24] H. Chen, S. Van Huffel, J. Vandewalle, Improved methods for exponential parameter estimation in the presence of known poles and noise, IEEE Trans. Signal Process. 45 (5) (1997) 1390–1393, http://dx.doi.org/10.1109/78.575717.